RESEARCH ARTICLE

NANO · MICRO small
www.small-journal.com

Designing Lithiophilic Lithium Metal Surface by a Hybrid Covalent Organic Framework and MXene Coating

*Osman Goni Shovon, Francis En Yoong Wong, and Junjie Niu**

With the increasing demand for developing large-energy-density and safe batteries, a reliable lithium metal as an anode becomes more and more important in various lithium metal and solid-state batteries. On the basis of better lithium regulation from MXene, a lithiophilic lithium metal surface is designed by introducing a 2D hybrid coating that consists of a thin covalent organic framework (COF-1) modified MXene layer (denoted as COF-MXene-Li). The abundant lithiophilic boroxine sites on 2D COF-1 attract lithium ions while the MXene further regulates lithium homogeneous nucleation and growth, thus preventing dendrite formation. The coin cell battery paired with $LiNi_{0.8}Mn_{0.1}Co_{0.1}O_2$ (NMC811) as cathode material displays 17% more capacity retention compared with pure lithium metal after 400 cycles at 0.5C.Over 81.4% capacity retention along with 99.96% Coulombic efficiency (CE) of a 1.0 Ah pouch cell versus $LiNi_{0.8}Co_{0.15}Al_{0.05}O_2$ (NCA) after 250 cycles is received. The assembled 1.6 Ah pouch cell with NMC811 show an energy density of up to 366.7 Wh Kg^{-1} and an actual energy density based on the whole cell of up to 339.7 Wh Kg^{-1}. The improved cycling stability particularly in pouch cells opens broad applications for this hybrid coating modified lithium metal as anode electrode in a variety of large-energy-density battery systems.

1. Introduction

Due to the high theoretical capacity of 3860 $mAhg^{-1}$ and low redox potential of −3.040 V versus standard hydrogen electrode, lithium metal is considered one of the most promising anode electrode candidates in next-generation lithium ion, lithium metal, lithium sulfur/air, and solid-state batteries.[1,2] However, challenges such as unstable solid electrolyte interphase (SEI), volume expansion, high chemical reactivity, and dendrite growth restrain its role in practical batteries.[3] In particular, un-even lithium deposition/extraction during the plating/stripping process ruptures the initial SEI, allowing the exposed fresh Li to continuously consume electrolyte to form thick SEI, leading to low CE and reduced cyclability. Moreover, Li preferentially nucleates and grows at the cracked SEI region, eventually developing into dendrites, which create a high safety issue of short circuits.[4] Thus seeking a strategy to regulate the lithium deposition/extraction and prevent the dendrite is critical for lithium metal anode electrodes.

To date a series of approaches to modifying Li/electrolyte interface such as replacing pure Li metal with Li-based alloy material,[5] applying a protective coating,[6] constructing an artificial SEI layer,[7] introducing lithiophilic seeds,[8] and optimizing electrolyte,[9,10] have been attempted. Recently an artificial SEI was created on Li metal by using ordered mesoporous zirconium oxophosphate, which promoted Li^+ ions flow during the initial electroplating process.[11] A covalent organic framework-based functional separator (COF@PP) was fabricated with the adhesion of TpPa-$2SO_3H$ COF nanosheets and 1D cellulose nanofibers to resolve the issue of disordered Li dendrite growth on Li metal.[12] Due to the high conductivity, better lithiophilicity, and mechanical robustness, recently the 2D layered Ti_3C_2 MXene exhibited great potential in lithium dendrite suppression. Zeng et al. developed a stoichiometric $Ti_3C_2T_x$ (S- $Ti_3C_2T_x$) MXene coating that provides plenty of nucleation sites, lowering the overpotential for Li nucleation and promoting more uniform Li plating, which reduces uncontrolled Li dendrite growth.[13] To achieve more controllable Li deposition with free dendrite, lithiophilic functional groups on MXene nanosheets need to be further investigated.[3]

Covalent organic frameworks (COFs) are a new polymer class with specific organic groups covalently connected to a periodic network, which have high surface areas, adjustable pore sizes/porosity, structural stability, and predictability, along with customized functionalities.[14] The scalable production of COFs by simple chemical reactions extends their applications in diverse fields such as photovoltaics, energy storage, gas storage, and catalyst supports.[15] The unique feature of well-defined lithiophilic sites displays promising roles in electrode materials of various batteries.[16] Song et al. combined COF-1 with graphene as a lithiophilic host to achieve long-cycling battery performance.[17] A new type of polyimide COFs was developed as anode coating, which showed a high density of ordered lithiophilic quinoxaline and phthalimide sites.[18] A fiber COF with numerous lithiophilic

O. G. Shovon, F. E. Y. Wong, J. Niu
Department of Materials Science and Engineering
CEAS
University of Wisconsin—Milwaukee Milwaukee
Wisconsin 53211, USA
E-mail: niu@uwm.edu

The ORCID identification number(s) for the author(s) of this article can be found under https://doi.org/10.1002/smll.202501769

DOI: 10.1002/smll.202501769

sites of aldehyde base and nitrogen groups improved Li^+ ions migration and uniform lithium deposition. The mesh-stacked fibrous polymer provided a buffering effect, effectively mitigating volume change during Li plating and stripping while reducing local current density.[19] Recently Zheng et al. reported a 3D COF as an anodic protective layer using 6-connected phosphazene and 4-connected porphyrin, which led to highly smooth and compact Li deposition.[20]

In our previous work, we designed an inter-layer-calated thin Li metal (ILC-Li) electrode using non-delaminated 2D $Ti_3C_2T_x$ MXene stacks coated on an ultra-thin Li host.[21] Recently we developed a dual-layer interphase that was composed of an organic lithium carbonate salt and a BF_3-doped monolayer MXene on the surface of lithium metal, which greatly enhanced the interfacial stability and thus reduced the SEI thickness.[22] The introduction of lithiophilic functional groups via heteroatom such as N, P, B, and O doping or dual heteroatom doping,[4] BN as an interfacial layer,[23] and MXene-BN introduced artificial SEI[24] can favor the homogeneous lithium deposition and improve the battery cycling performance. In contrast to graphene, MXene has better lithiophilicity with a lithium binding energy of −2.93 eV.[25] In this article, we developed a reliable Li metal surface named COF-MXene-Li by covering a thin hybrid coating that consists of 2D lithiophilic COF-1 and conductive MXenes. The plenty of favorable Li sites among the COF-1 and excellent electronic conductivity along the layered MXenes led to form a uniform Li film by reducing the nucleation barrier and inhibiting dendrite formation. As a result, a thin SEI layer with ≈6 nm organic and ≈90 nm inorganic layers was achieved. The improved surface stability greatly extended the battery cycling performance, particularly in large-capacity pouch cells.

2. Results and Discussion

To form the COF-MXene-Li, multilayer Ti_3C_2 MXene was first obtained by etching MAX precursor with hydrofluoric acid (HF).[21,26] Subsequently, a diluted suspension of purified MXene in tetrahydrofuran was prepared after a series of treatments. The COF-1 was synthesized by heating 1,4-benzenediboronic acid (BDBA) in a mesitylene-dioxane solution.[17,27] The well-defined and ordered framework of the as-received COF-1 was confirmed by using powder X-ray diffraction (XRD) (Figure S1, Supporting Information). Then the COF-MXene hybrid composite was formed via a solvothermal method. In the final step, the received hybrid dispersion was spray-coated on a Li metal surface (**Figure 1**a). Scanning electron microscopy (SEM) surface morphologies of the pure Li metal (Figure 1b), COF-MXene-Li (Figure 1c), and COF-MXene-Cu (Figure S2, Supporting Information) show that the hybrid COF-MXene composite coating was intimately covered on the Li metal and Cu surfaces. It is evident that smooth channels and improved storage sites can be provided by the pore structure for lithium-ion migration.[28] So, the porous configuration from both 2D COF-1 and MXene ensures sufficient active sites and spaces to accommodate lithium deposition.

The wetting performance of the surface with carbonate-based electrolyte and molten lithium was checked. As observed in Figure 1d, the contact angle (CA) of the electrolyte on pure Li metal is 33°, which is much higher than 11° of COF-MXene-Li. Similarly, the pure Li metal showed a high CA of 134° with molten lithium while the COF-MXene-Li only delivered a small CA of 69° (Figure 1e). The clearly reduced CA of both electrolyte and molten lithium on the COF-MXene-Li (Table S1, Supporting Information) and stable surface morphology (Figure S3, Supporting Information) indicates an improved surface wetting performance, which can facilitate wide and uniform distribution of Li ions. It is believed that the increased lithiophilicity from the hybrid composite, especially from the COF-1 contributed to this behavior.[17]

X-ray photoelectron spectroscopy (XPS) was used to examine the chemical composition of the samples. The C 1s peaks with a strong C—C binding at 284.8 eV (Figure 1f) and Ti 2p (Figure 1 h) peaks with a comparatively weak titanium oxide binding at 458.7/464.2 eV confirmed the Ti_3C_2 MXene structure (Figure S4a, Supporting Information).[21] Compared with pure COF-1, the COF-MXene hybrid composite exhibited two new B 1s peaks at 191.2 and 193.3 eV, which correspond to BC_2O and BCO_2 respectively,[22,29] along with a peak of boronic acid group, $B(OH)_2$ at 191.9 eV and the B_3O_3 peak (Figure 1i).[30] The B_3O_3 group as shown in the O 1s peak at 533.1 eV and the B 1s peak at 192.0 eV were from the COF-1[17] (Figure S4b, Supporting Information) while the new covalent bindings of BC_2O and BCO_2 were generated by the reaction between COF-1 and MXene. In order to further check the reaction with lithium, the samples of pure Li metal (Figure S5a, Supporting Information), MXene (Figures S5b and S6, Supporting Information), COF-1 (Figure S7a), and COF-MXene (Figures S7b and S8, Supporting Information) coated on lithium metal surface were measured respectively. As seen from the obtained XPS spectra, no new peaks appeared, indicating a non-covalent, Van der Waals binding of the hybrid composite with the lithium host.

The component and thickness of the SEI layer are critical in determining the uniform lithium deposition/extraction with zero dendrite formation as well as the battery cycling capability and energy density.[31] The SEI information of the COF-MXene-Li electrode upon stripping after five cycles in a symmetric cell was revealed by using X-ray photoelectron spectroscopy (XPS) depth profiles (**Figure 2**). As observed from the Li 1s peak in Figure 2 and Figure S9 (Supporting Information), various inorganic compounds including LiF, Li_2CO_3/LiOH, and Li_2O were identified. The size of the inorganic-rich layer was estimated on the basis of a lithium mole ratio of less than 60%.[21] It was found that the inorganic layer thickness of the COF-MXene-Li electrode was ≈90 nm, which was much thinner than ≈270 nm of the pure Li metal electrode (Table S2, Supporting Information). The organic component of the SEI layer was revealed by the C 1s peak of C—C binding at 284.8 eV, C—O binding at 286.7 eV, C═O binding at 287.8 eV, and the O 1s peak at 530.4 eV.[22] The size of the organic layer was estimated by following the evolution of CF_3 peak in F 1s. It was observed that the CF_3 binding at 688.1 eV with COF-MXene-Li electrode disappeared after etching 20 s (Figure 2), indicating a thin organic-rich thickness of ≈6.0 nm (Table S2, Supporting Information). As a comparison, a large CF_3 peak with pure Li metal electrode remained even after etching 60 s (Figure S9, Supporting Information), showing a much thicker organic-rich layer of more than 18.0 nm (Table S2, Supporting Information). The COF-MXene layer on the Li metal surface was confirmed by the B 1s peaks at 191.2, 191.9, 192.0, and 193.3 eV that

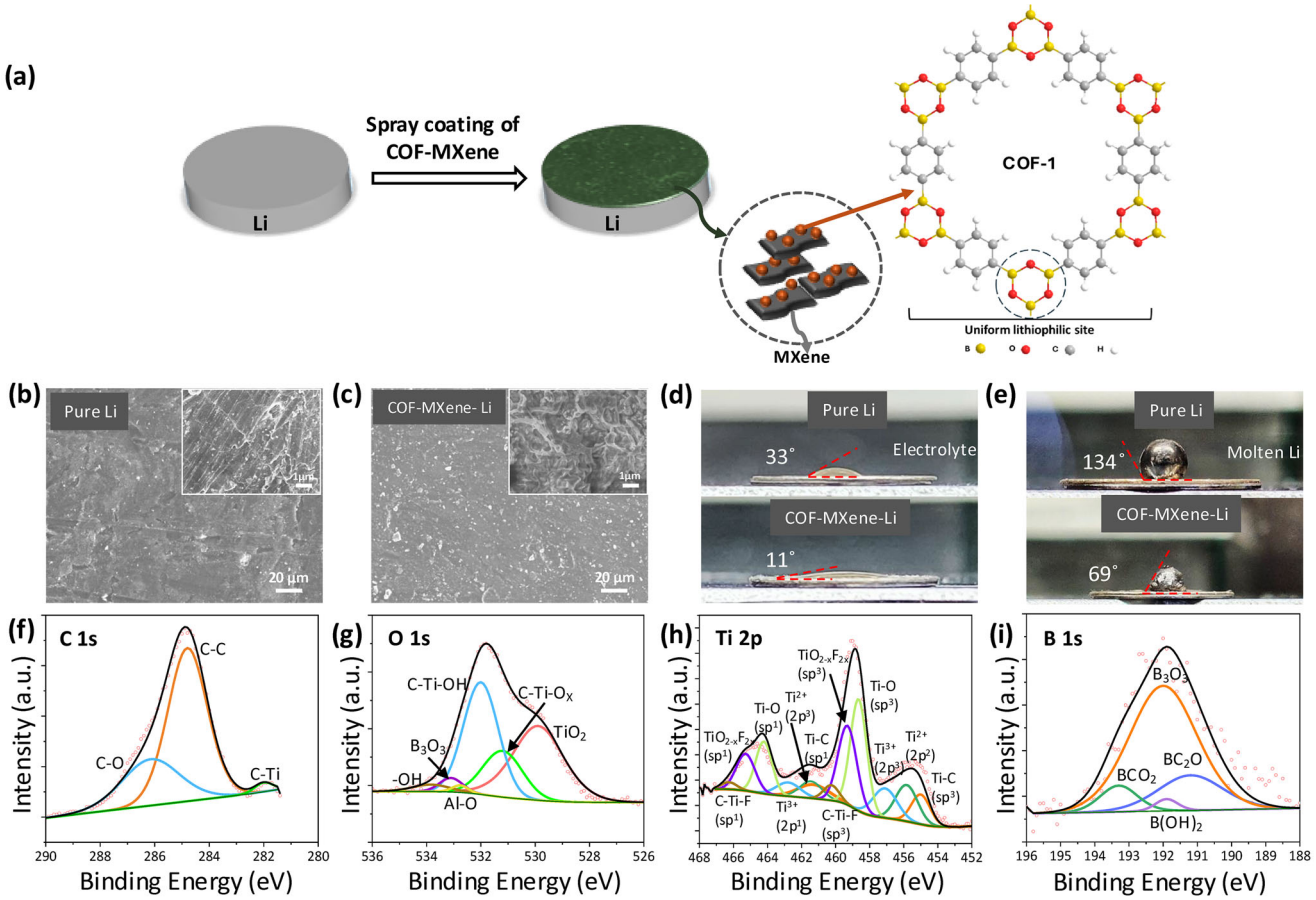

Figure 1. Design COF-MXene modified Li metal surface. a) Synthesis of the COF-MXene-Li. SEM morphologies of b) pure Li and c) COF-MXene-Li surfaces. The insets are enlarged images. Contact angles of d) electrolyte and e) molten Li on pure Li (top) and COF-MXene-Li (bottom). XPS spectra of the f) C 1s, g) O 1s, h) Ti 2p, and i) B 1s of the COF-MXene layer on Cu foil.

are associated with BC_2O, $B(OH)_2$, B_3O_3, and BCO_2 (Figure 2, B 1s), which is in agreement with the COF-MXene results in Figure 1i. In addition, The Ti—C bonding at 282.1 eV in C 1s peaks and Ti—O bonding at 529.9 eV in O 1s peaks with the COF-MXene-Li electrode were detected after etching 60 s, confirming the MXene layer on the surface (Figure 2).

It is known that pure Li metal keeps consuming electrolytes by forming a thick SEI layer (**Figure 3a**). The covalent organic framework, COF-1, has a strong affinity to lithium, resulting in a high lithiophilicity.[3,17] The boron atoms in B_3O_3 (boroxine) sites are electron-deficient, which facilitates Li valence electrons to transfer to the boron atom of boroxine, making them attractive to Li^+ ions. The lone pairs of electrons on the oxygen atoms in the boroxine sites allow them to preferably coordinate with Li^+ ions. Such coordination sites improve lithiophilicity, which can stabilize Li^+ ions transport inside the framework (Figure 3b).[32,33] In parallel, COF-1 has a large surface area of 288.2 m^2g^{-1} and highly porous network (Figure S10, Supporting Information), which greatly enhanced the electrolyte wettability (Figure 1d). The better wettability among the submicron level pores and channels reduces the Li^+ ion transport distance from electrolyte to active material and mitigates the polarization effects. In addition, COF-1 with staggered AB stacking displays a stable configuration with more interlayer spaces which is favorable for Li^+ ions intercalation (Figure 3c).[27]

Moreover, MXene ($Ti_3C_2T_x$ MXene, T_x stands for surface termination) displays a high electrical conductivity, ranging from 3×10^3 to over 15×10^3 Scm^{-1},[34] which is beneficial to maintain uniform current distribution across the lithium metal surface. As contrast, COF-1 exhibits a relatively lower electrical conductivity,[35] which shows moderate lithium regulation by reducing uneven nucleation and minimizing the undesirable side reactions between the active lithium surface and electrolyte. On the basis of the conductive MXene backbone and flexible COF-1 layer, a reduced reaction of organic and inorganic products with electrolytes was achieved, which preserves the integrity of SEI during long cycling.[36] As shown in Figure 3d, on the basis of XPS depth profile, the electrode with COF-MXene-Li showed a ≈6 nm organic layer and a ≈90 nm inorganic layer, which were both thinner compared with the pure Li metal electrode of ≈36 and ≈270 nm.

The synergistic interaction between high-mechanical-strength COF-1 and MXene contributes to the improved volume accommodation upon cycling. MXene has excellent mechanical strength with Young's modulus of ≈330 GPa.[37] The Young's modulus of COF-1 is ≈33 GPa,[38] which can provide further

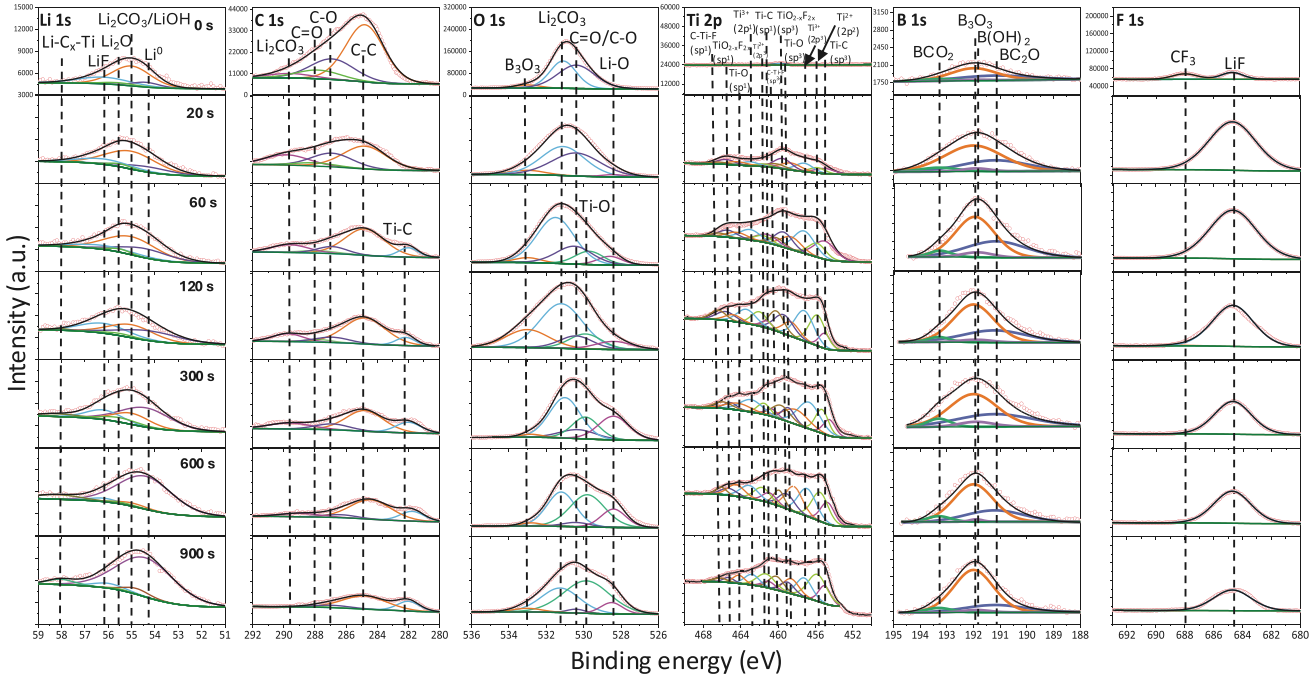

Figure 2. SEI composition analysis of a symmetric cell by using XPS depth profile. The COF-MXene-Li as an electrode was measured upon stripping after five cycles. The current density was 1.0 mAcm^{-2} and the capacity was 1.0 mAhcm^{-2}.

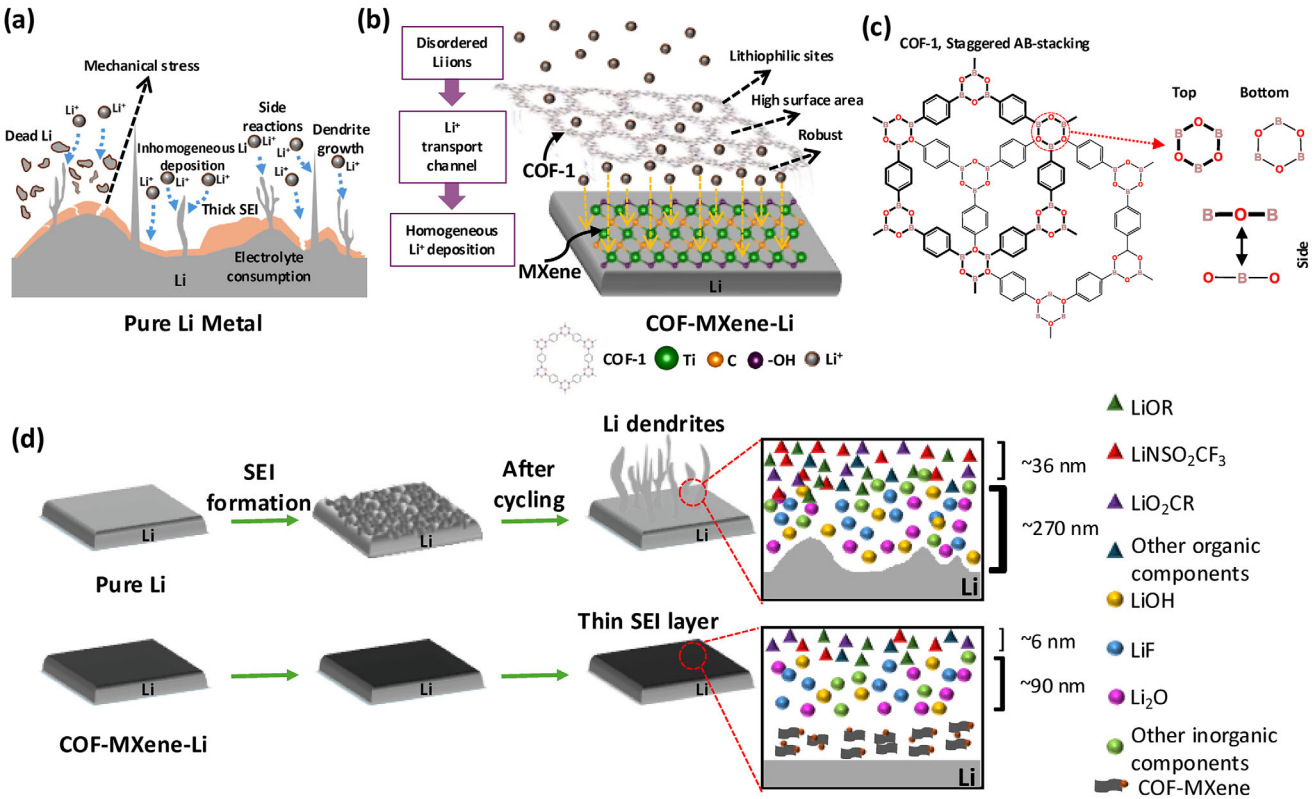

Figure 3. SEI configuration with pure Li metal and COF-Mxene-Li. Schematic diagram of the interface on a) pure Li metal and b) COF-MXene-Li. c) Staggered AB-stacking of as-synthesized COF-1. Top and side views show the top and bottom layers cross each other. d) Component anatomy based on XPS depth profiles of pure Li metal and COF-MXene-Li upon stripping after five cycles in a symmetric cell.

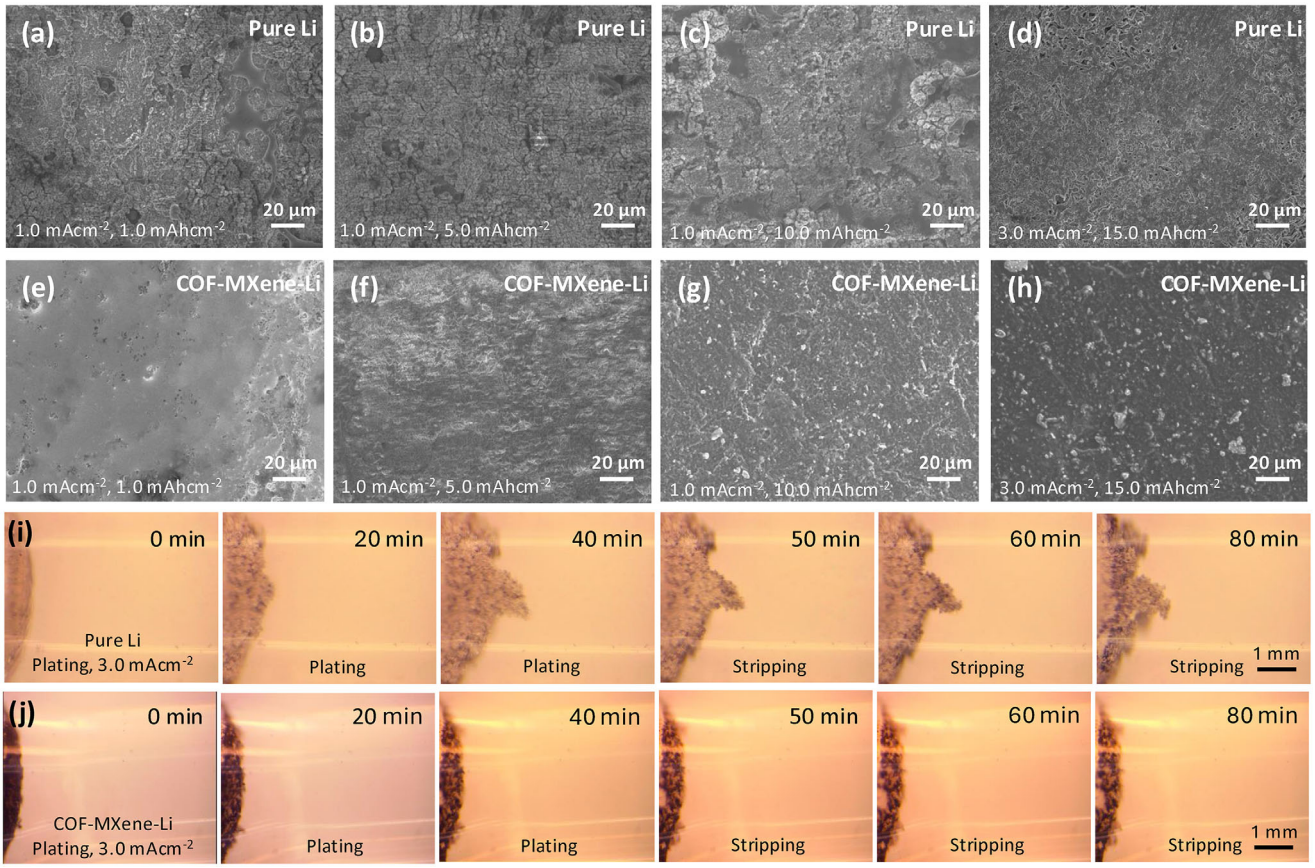

Figure 4. Surface morphology evolution of lithium metal electrode in symmetric cells. SEM morphologies of pure Li metal a–c) under a current density of 1.0 mAcm^{-2} after plating for 1, 5, and 10 h, and d) under a current density of 3.0 mAcm^{-2} after plating for 5 h. SEM morphologies of COF-MXene-Li e–g) under a current density of 1.0 mAcm^{-2} after plating for 1, 5, and 10 h, and h) under a current density of 3.0 mAcm^{-2} after plating for 5 h. In situ observation of the mossy/dendritic Li during plating (0–40 min) and stripping (40–80 min) with i) pure Li and j) COF-MXene-Li inside a capillary cell. The current density: ≈3.0 mAcm^{-2}.

reinforcement to regulate the lithium deposition and resist the dendrite growth pressure of 2–4 GPa[39] through its strong covalent network without losing its structural integrity. In addition, the expanded interlayer space and parallelly aligned layer among the MXene restrict the Li growth along the perpendicular direction and lead to a horizontal growth of lithium on Li metal surface.[21,40] As a result, the continuous crack and failure of SEI are reduced, leading to a uniform lithium deposition/extraction with suppressed dendrite (Figure 3).[22]

The surface morphology evolution of the electrode upon cycling was investigated in symmetric cells. It was observed that uneven lithium deposition with increased mossy/dendritic lithium was formed on pure Li metal when increasing the plating capacity (**Figure** 4a–c) and current density (Figure 4d). In contrast, the COF-MXene-Li displayed a comparatively smooth surface under both current densities of 1.0 mAcm^{-2} (Figure 4e–g) and 3.0 mAcm^{-2} (Figure 4 h). The real-time mossy/dendritic Li growth/depletion upon lithium plating and stripping at 3.0 mA cm^{-2} was studied in a capillary cell. As seen in Figure 4i, a clear mossy/dendritic lithium appeared on the pure Li metal electrode only after 20 min plating and remained even after stripping. However, a homogenous lithium deposition/depletion free of mossy/dendritic lithium on the COF-MXene-Li electrode was found during the plating (0–40 min) and stripping (40–80 min) (Figure 4j). It is known that the non-homogeneous lithium nucleation/growth can generate dendrites which cause short-circuit safety concerns.[17,36] Further, the highly active lithium dendrite can accelerate side reactions with electrolytes, leading to low Coulombic efficiency and short cycling performance. With our modified electrode, both the lithiophilic COF-1 and conductive MXene resulted in a low lithium nucleation barrier and better volume accommodation, which contributed to the uniform Li deposition with relieved dendrite growth. The reversible deposition and dissolution of lithium can also be observed from the cross-section evolution upon plating and stripping (Figure S11, Supporting Information).

The electrochemical property of the full-cell battery paired with $LiNi_{0.8}Mn_{0.1}Co_{0.1}O_2$ (NMC811) was investigated by cyclic voltammetry (CV) (**Figure** 5a). It was found that the battery with COF-MXene-Li displayed sharper and stronger redox peaks compared to the pure Li metal. In addition, the potential variation of the phase transformation between hexagonal and monoclinic (H1-M) phases was reduced. These results indicate enhanced Li^+ diffusion kinetics.[39] The interface resistance between the electrode and electrolyte was checked by using electrochemical impedance spectroscopy (EIS) in both symmetric and full cells. Both

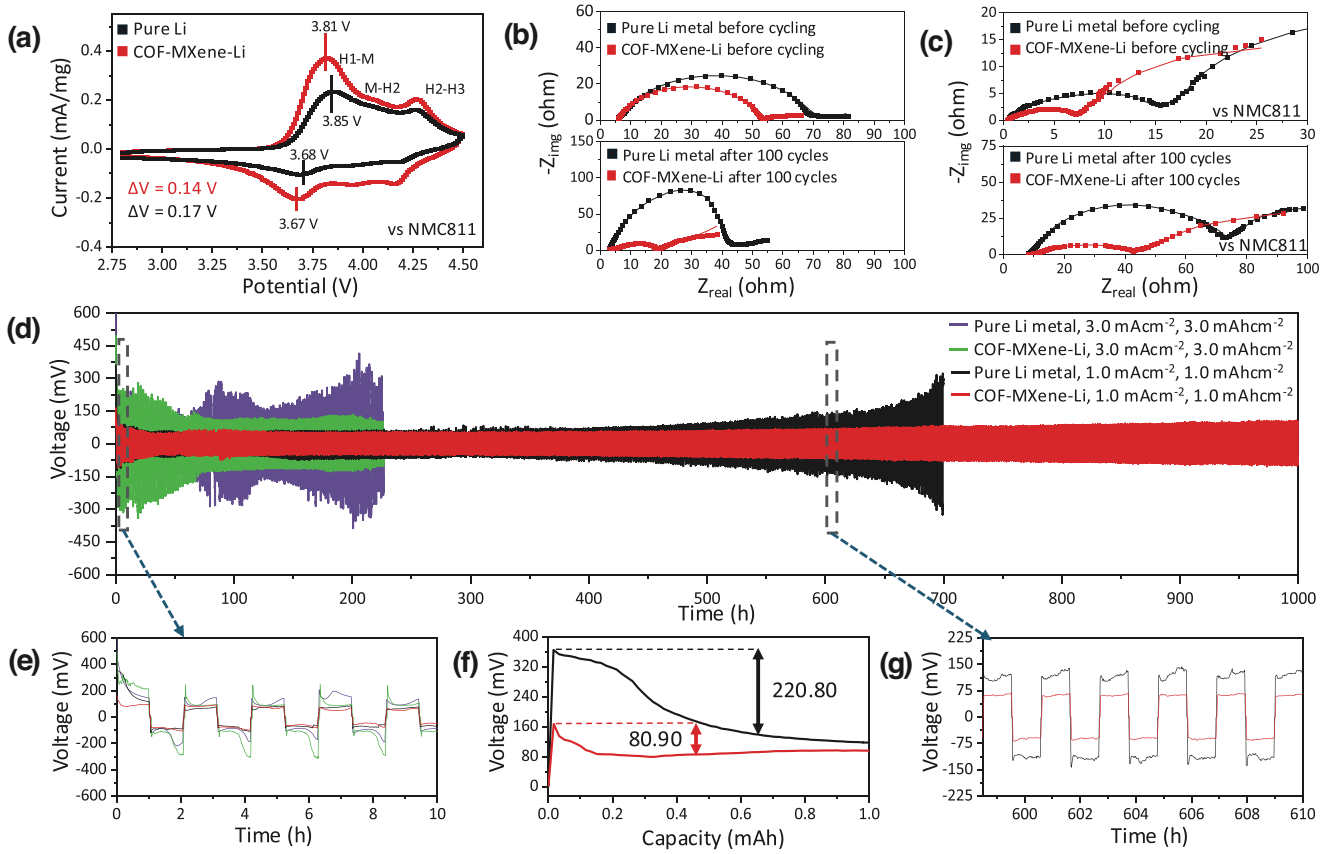

Figure 5. Electrochemical property of the battery with COF-MXene-Li as an electrode. a) CVs of the battery paired with NMC811 as cathode material. b) Nyquist plots of pure Li metal and COF-MXene-Li before and after 100 cycles in symmetric cells. c) Nyquist plots of pure Li metal and COF-MXene-Li before and after 100 cycles at 0.5C in a full battery paired with NMC811 as cathode material. d) Galvanostatic cycling of symmetric cells with pure Li metal and COF-MXene-Li metal at 1.0 mAcm^{-2}, 1.0 mAhcm^{-2}, and 3.0 mAcm^{-2}, 3.0 mAhcm^{-2}. e) The enlarged voltage profiles of 0–10th h. f) The voltage profile of the 1st cycle at 1.0 mAcm^{-2}, 1.0 mAhcm^{-2}. g) The enlarged voltage profiles of 600–610th h.

symmetric cells exhibited a similar contact resistance of ≈5.9 Ω, while the cell with COF-MXene-Li exhibited a reduced transfer resistance of ≈45.7 Ω in contrast to 60.4 Ω with pure Li metal before cycling (Figure 5b). After 100 cycles, the transfer resistance with COF-MXene-Li was further decreased to ≈14.4 Ω, which is much smaller than 36.6 Ω of the pure Li metal. In the full cell with NMC811, a lower transfer resistance with COF-MXene-Li was also obtained before and after cycling (Figure 5c). It is believed that the reduced transfer resistance with COF-MXene-Li was attributed to the reduced SEI layer on the interface as confirmed by the XPS depth profiles in Figures 2 and 3d.[21] In addition, the diffusion kinetics of Li^+ was investigated via EIS measurement in symmetric and full cells (Figures S12 and S13, Supporting Information). As seen from the relationship between real impedance (Z_{real}) and the inverse square root of angular frequency ($\omega^{-0.5}$) in the low-frequency region, the slope of COF-MXene-Li was smaller than pure Li before and after cycling, which indicates a fast Li^+ diffusion kinetics.[41]

The electrochemical stability of the Li metal electrodes during plating and stripping in symmetric cells is shown in Figure 5d. The cell with COF-MXene-Li displayed an initial overvoltage of 88.5 mV, whereas the cell with pure Li showed a higher value of 154.7 mV at a current density of 1.0 mA cm^{-2} (Figure 5d,e). As revealed in Figure 5f, a low lithium nucleation overvoltage of 80.9 mV appeared, which was much lower than 220.8 mV with the pure Li metal. This reduced nucleation energy barrier can facilitate preferred lithium deposition, leading to forming a homogeneous lithium film. The overvoltage with COF-MXene-Li was stabilized at 92.0–105.0 mV up to 1000 h under 1.0 mA cm^{-2} and 96.0–107.0 mV up to 225 h under 3.0 mA cm^{-2}, which were lower than the pure Li metal (Figure 5d–g) and MXene coated Li metal (Figure S14, Supporting Information). In particular, the cell with pure Li metal showed an initial overvoltage of ≈180.4 mV and reached 270 mV only after 90 h at 3.0 mAcm^{-2} (Figure 5d,e). The greatly reduced overvoltage upon long cycling due to the synergetic interaction of COF-1 and MXene indicates that COF-MXene-Li has a promising performance in forming homogenous lithium film during charging/discharging.

Battery performance of full coin cells versus NMC811 and pouch cells versus $LiNi_{0.8}Co_{0.15}Al_{0.05}O_2$ (NCA) were respectively investigated. As shown in **Figure 6a**, the battery with COF-MXene-Li displayed an initial capacity of 205.1 mAhg^{-1} with a CE of 86.5% at 0.1C. A high-capacity retention of 137.7 mAhg^1 after 400 cycles at 0.5C remained, which was much higher than the capacity of 102.4 mAhg^{-1} with pure Li metal. Under a high charge/discharge rate of 1.0C after 3 cycles at 0.1C, the cell with

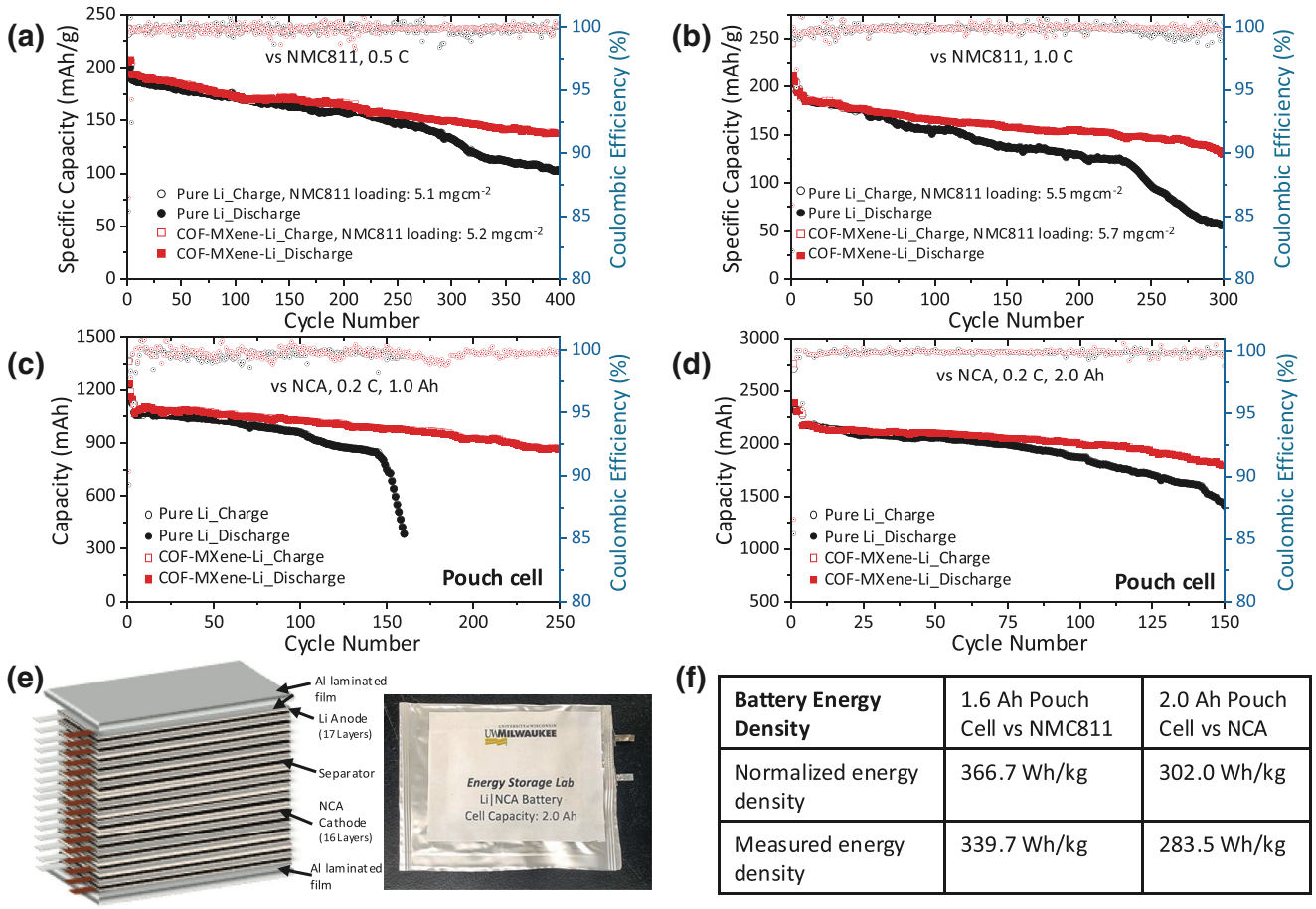

(f)

Battery Energy Density	1.6 Ah Pouch Cell vs NMC811	2.0 Ah Pouch Cell vs NCA
Normalized energy density	366.7 Wh/kg	302.0 Wh/kg
Measured energy density	339.7 Wh/kg	283.5 Wh/kg

Figure 6. Battery performance with COF-MXene-Li as anode material. Coin cell battery cycling performance versus NMC811 as cathode material a) at 0.5C, and b) at 1.0C. The battery was activated at 0.1C for three cycles. Pouch cell performance paired with NCA at 0.2C with a capacity of c) 1.0 Ah, and d) 2.0 Ah. e) Schematic illustration and photo of the assembled pouch cell with modified Li metal as anode and NCA as a cathode. f) Normalized and measured energy density of the pouch cells coupled with COF-MXene-Li as anode, NMC811, and NCA as cathode electrode material. The measured energy density was calculated on the basis of the actual weight of the whole battery and capacity.

COF-MXene-Li exhibited an initial discharge capacity up to 196.4 $mAhg^{-1}$ with a CE of 96.7%, which was higher than the 194.7 $mAhg^{-1}$ with a CE of 95.2% (Figure 6b). After 300 cycles, the cell with COF-MXene-Li still showed a capacity of 129.4 $mAhg^{-1}$ with 66.0% capacity retention while the cell with pure Li metal dropped to 56.4 $mAhg^{-1}$ with only 29.0% capacity retention. The validated battery cycling performance in large-capacity pouch cell batteries paired with NCA exhibits promising potential in broad applications in a variety of energy-storage devices (Figure 6e). It was found that the pouch cell with COF-MXene-Li maintained a reliable capacity of 868.6 mAh with ≈81.4% capacity retention after 250 cycles (Figure 6c). In contrast, the battery with pure Li metal exhibited a fast capacity decay to 383.4 mAh after only 160 cycles. Under the higher capacity of 2.0 Ah, the battery with COF-MXene-Li displayed a capacity of 1797.8 mAh with a capacity retention up to 82.6% after 150 cycles (Figure 6d). However, the battery with pure Li metal decreased to 1413.3 mAh with only 65.1% capacity retention. The assembled 1.6 Ah pouch cell versus NMC811 with a low E/C ratio of 1.9 gAh^{-1} showed a normalized energy density of 366.7 Wh Kg^{-1} and a measured energy density of 339.7 Wh Kg^{-1} on the basis of whole cell-pack weight (Figure 6f; Figure S15 and Table S4, Supporting Information). The performance comparison with select lithium metal-based anodes is shown in Table S5 (Supporting Information). In addition, the 2.0 Ah pouch cell versus NCA with a E/C ratio of 3.0 gAh^{-1} demonstrated a normalized energy density of 302.0 Wh Kg^{-1} and the measured energy density of 283.5 Wh Kg^{-1} (Figure 6f). The enhanced energy density in pouch-cell batteries shows great applications in extending working time in various electronic devices and electric vehicles.

Battery performance of Li/Cu half-cells was also performed with pure Cu and COF-MXene-Cu. As seen from Figure S16 (Supporting Information), a higher and more stable Coulombic efficiency with COF-MXene-Cu electrode was received, which indicates a smooth lithium plating/stripping process and thin SEI formation with a low interface impedance.[42] The improved electrochemical property and battery performance benefited from the synergetic interaction of the conductive 2D MXene and lithiophilic COF-1. It has been reported that the doped monolayer MXene allows lithium deposition along the horizontal direction.[22] In parallel, the sufficient lithiophilic boroxine sites among the COF-1 attract more Li^+ ions from the electrolyte, which promotes

uniform lithium nucleation and growth, thus preventing the possible dendrite formation.

3. Conclusion

Due to the large theoretical capacity, low electrochemical potential, and lightweight, lithium metal is one of the most promising anodes in large energy-density liquid and solid-state batteries. Challenges of uncontrolled Li dendrite formation, high chemical reactivity, and unstable solid electrolyte interphase limit its practical applications. In this work, we successfully developed a hybrid thin protective layer on the surface of lithium metal by using 2D COF-1 and Ti_3C_2 MXene. The existing lithiophilic boroxine sites on COF-1 with high electrolyte wetting promoted lithium-ion transport and reduced the nucleation barrier, leading to a homogenous Li deposition and extraction. In addition, the synergistic interaction between the low-conductivity polymer and high-conductivity MXene regulated lithium growth and thus suppressed the dendrite generation. As a result, a reduced overvoltage after cycling 1000 h in symmetric cells was obtained. The full coin cell battery displayed high-capacity retention after long cycling at high rates. The lab-scale 1.6 Ah pouch cell displayed a high energy density of 366.7 Wh Kg^{-1}. The strategy to modify the lithium metal surface using lithiophilic covalent organic framework and 2D MXene offers a pathway toward a high-energy-density battery system with high reliability and sustainability. Future research will focus on scaling up the modified Li metal anode in various electrolyte systems, as well as pairing it with different advanced cathode materials to fully utilize the high capacity of lithium metal-based batteries.

4. Experimental Section

Synthesis of COF-MXene-Li: Ti_3C_2 MXene was synthesized by etching Ti_3AlC_2 MAX (400 mesh, Lizhou Kai Kai Ceramic Materials) via hydrofluoric acid (HF, 48–52%, Sigma–Aldrich).[26] Typically 3.0 g of MAX precursor was slowly added to 30.0 mL of HF solution in a Teflon container (Baoshishan) and continuously stirred with a magnetic stirrer (RT Basic-17, Thermo Scientific). After stirring for 1 h at room temperature, the container was placed in a water bath (Symphony, VWR) and stirred at 60 °C (Stirring Hot Plate, Thermo Scientific Cimarec). After 24 h, the MXene sediment was filtrated by centrifuge (Compact Centrifuge, model 6755, Corning LSE) and washed with de-ionized (DI) water (Purelab) until the pH reached 6.0 (pH Test Strips, VWR Chemicals BDH). Finally, the MXene sample was collected using a vacuum-assisted filtration (Vacuum Filtration System, VWR) with a 0.22 µm pore size polyvinyl difluoride (PVDF) filter membrane (EZ Flow, 364-2612-OEM) and dried in a vacuum oven (Ai 0.9, Across International) at 80 °C for 24 h.

A diluted MXene dispersion was prepared based on the previous work.[22] 0.1 g MXene was dispersed in a 25 wt.% tetrabutylammonium hydroxide solution (40% in water, Sigma–Aldrich) and stirred for 6 h at room temperature. The obtained solution was first filtrated by centrifuge and rinsed three times with ethanol (200 proof, Decon Labs). Then the sample was dispersed in 50.0 mL of tetrahydrofuran (THF, anhydrous, 99.9%, Sigma–Aldrich) solvent. After agitating for 10 h in an ultrasound cleaner (Symphony, VWR), the final MXene sample was collected by centrifuge.

The COF-MXene hybrid coating was prepared by using a solvothermal method.[17,27] In a typical experiment, 3.0 wt.% of 1,4-benzenediboronic acid (BDBA; 98%, Alfa Aesar) was mixed with MXene sample in a mixture solution of 20.0 mL mesitylene (99%, Sigma–Aldrich) and 20.0 mL 1,4-dioxane (99%, Sigma–Aldrich). After agitating for 20 min in the ultrasound cleaner and stirring for 15 min, the solution was transferred to a stainless-steel autoclave reactor lined with Teflon (Baoshishan). The reactor was then kept at 125 °C for 72 h. The hybrid sample was obtained through centrifugation (Compact Centrifuge, model 6755, Corning LSE). After rinsing three times by THF, the sample was dried in a vacuum oven (Ai 0.9, Across International) at room temperature for 24 h.

Before coating on the lithium metal surface, the COF-MXene sample was dispersed in THF and agitated in the ultrasound cleaner for 30 min. The Li metal coating was completed inside an Ar-filled glovebox (H_2O < 0.5 ppm, O_2 < 0.1 ppm, Mbraun Labstar Pro). Before coating, the pure Li foil (for coin cells, diameter: 15.6 mm, thickness: 0.25 mm, 99.9%, MSE Supplies; For pouch cells, thin lithium on Cu, Li thickness: 40 µm, Cu: 10 µm, ≥99.9% purity, MSE Supplies) was carefully cleaned with a soft brush to remove surface contamination. The as-prepared COF-MXene solution was sprayed on Li metal surface with a solution-to-area ratio of ≈45 µL cm^{-2} (≈0.09 mg cm^{-2}) by using a sprayer (Amazon). The final COF-MXene-Li was obtained after drying at room temperature for 24 h. COF-MXene-Cu was also prepared with the same coating process.

Coin Cell Assembly: The electrochemical property and battery cycling performance were tested using symmetric and coin cells (CR2032, Xingye Co., Ltd.). Symmetric cells were assembled by using pure Li foil or COF-MXene-Li as both anode and cathode electrodes in the Ar-filled glovebox (H_2O < 0.5 ppm; O_2 < 0.1 ppm, Mbraun, Labstar Pro). The electrolyte was 1.0 M lithium bistrifluoromethane sulfonimide (LiTFSI, BASF Corp.) in 1,3 dioxolane/DME (BASF Corp.) with a 1:1 volume ratio, with an addition of 0.1 M $LiNO_3$ (99.99%, Sigma–Aldrich). The electrolyte amount was ≈50 µL in each coin cell.

For Li/Cu half coin cells, the electrolyte was 1.0 M $LiPF_6$ (battery grade, >99.99% trace metals basis, Sigma–Aldrich) in a solvent consisting of ethylene carbonate (EC) (battery grade, BASF Corp.) and ethyl methyl carbonate (EMC) (battery grade, BASF Corp.) with 3:7 volume ratio, 2 wt.% vinylene carbonate (VC) (99.5%, battery grade, Sigma–Aldrich) and 10 wt.% Fluoroethylene carbonate (FEC) (99.8%, Santa Cruz Biotechnology Inc.). For regular full coin cells, the pure Li metal or COF-MXene-Li was used as the anode electrode and NMC811 as the cathode electrode material. The cathode electrode material slurry was prepared by mixing 80 wt.% NMC811 (Tap density: ≥2.1 g cm^{-3}, pH ≤11.80, BET Specific Surface Area: 0.6 ± 0.3 m^2g^{-1}, MSE Supplies) as active material, 10 wt.% conductive carbon black (SuperP C65, Timcal), and 10 wt.% polyvinylidene fluoride (PVDF, laboratory grade, Alfa Aesar) as the binder in N-methyl-2-pyrrolidinone (NMP, 99.9%, Headspace Solvents, Honeywell) solvent. Then the mixed slurry was coated on a 15 µm thick carbon-coated aluminum foil (99.3%, MTI Corp.) via film casting doctor blade and dried at 60 °C for 12 h in a vacuum oven (Vacuum oven, Ai 0.9, Across International). The received electrode was pressed under ≈10 MPa using a benchtop hydraulic press (Northern Tool+ Equipment), and then it was cut into circle discs by a disc cutter (MSK-T-07, MTI Corp.). The coin cell was assembled by pressing at ≈6 MPa inside an argon-filled glovebox using the as-prepared cathode electrode, polyethylene separator (Celgard 2400), and pure Li foil or the COF-MXene-Li as anode electrode. The electrolyte was 1.0 M $LiPF_6$ in a solvent consisting of EC and EMC with a 3:7 volume ratio, 2 wt.% VC, and 10 wt.% FEC.

Pouch Cell Assembly: Full pouch cells with a total capacity of 1.0 and 2.0 Ah were assembled using commercial NCA material as cathode electrode material. The double-side coated NCA electrode was obtained from a brand-new 18650 Samsung 35E battery with an active material loading of 41.0 mg cm^{-2} for double sides and the area of the electrode was 4 × 5 cm^2. During the assembly, nine layers (for 1.0 Ah) and sixteen layers (for 2.0 Ah) of double-side side coated NCA electrode were coupled with ten layers (for 1.0 Ah) and seventeen layers (for 2.0 Ah) of pure Li metal or COF-MXene-Li (The Li metal host: Li thickness: 40 µm, Cu: 10 µm, MSE Supplies). The 1.6 Ah full pouch cell using commercial NMC811 as cathode electrode material was also checked. Double-side coated NMC811 electrodes with an active material loading of 37.06 mg cm^{-2} for double sides and an area of 4.0 × 5.0 cm^2 were made before assembly. During the assembly, ten layers of double-side and two layers of single-side coated NMC811 as cathode were coupled with eleven layers of COF-MXene-Li as anode. The Celgard 2400 microporous polyethylene (PE) membrane was used as the separator. The Ni and Al tabs with 3 mm width (MTI Corp.) were used for anode and

cathode connections via an ultrasonic metal spot welding machine (TMAX-USW-2000 W, 40 Hz, TMAX Battery Equipment). The electrolyte was 1.0 M $LiPF_6$ (battery grade, >99.99% trace metals basis, Sigma–Aldrich) in a solvent consisting of ethylene carbonate (EC) (battery grade, BASF Corp.) and ethyl methyl carbonate (EMC) (battery grade, BASF Corp.) with 3:7 volume ratio, 2 wt.% vinylene carbonate (VC) (99.5%, battery grade, Sigma–Aldrich) and 10 wt.% fluoroethylene carbonate (FEC) (99.8%, Santa Cruz Biotechnology Inc.). The cell was finally sealed by a pouch-cell vacuum sealing machine (TMAX-YF, TMAX Battery). During testing, all the pouch cells were kept in a clamping device with an external pressure of ≈172 kPa (25 psi).

Capillary Cell Assembly: The capillary cell was assembled by using a sealed transparent hourglass-type tube. The inner diameter of the middle part for observation was 3 mm, which was connected to two sides of the tube with a diameter of 4 mm. A symmetric cell with pure Li metal or COF-MXene-Li as electrodes was well sealed inside the capillary cell in the Ar-filled glovebox. A copper wire with a diameter of 1.0 mm (99%, Fisher Scientific) served as a current collector which was connected to the battery tester. The electrolyte was 1.0 M $LiPF_6$ in the solvent of EC and EMC with a 3:7 volume ratio, with 2 wt.% VC and 10 wt.% FEC as additives. A digital trinocular stereo zoom microscope (SM-3TZ-54S-5 M, AmScope) was used to record the surface morphology change upon Li stripping/plating by using a battery tester system (LANDT 2001CT, Landt Instruments, Inc.).

Electrochemical Property and Battery Performance Measurements: Gamry 600+ Potentiostat/Galvanostat/ZRA was used to check the EIS with a frequency range of 0.01–10^5 Hz. The EIS of symmetric cells was checked upon stripping after cycling. The EIS of the full cell with NMC811 was measured at a charged state of 4.3 V. The galvanostatic cycling performance of the assembled batteries after resting was measured by a battery tester system (LANDT 2001CT, Landt Instruments, Inc.). The cycling performance of the symmetric cells was checked under current densities of 1.0 and 3.0 mA cm^{-2}, respectively. All full coin cells and pouch cells were subjected to activation of charge/discharge cycles at 0.1C with a voltage range of 2.65–4.2 V for NCA and 2.8–4.3 V for NMC811.[43]

Sample Characterizations: For the characterization of the surface morphology evolution of samples, Hitachi S4800 ultrahigh resolution field emission scanning electron microscopy (FESEM) was used. SEM images were obtained at an acceleration voltage of 5.0 kV. Bruker D8 Discover X-ray Diffractometer using Ni filtered Cu Kα radiation with applied current and voltage of 40 mA and 40 kV, respectively was used to measure X-ray diffraction (XRD). The surface area, pore volume, and pore size of the samples were measured by using N_2 sorption/desorption isotherms with a Micromiritics ASAP 2020 system at 77 K and calculated by BET method. X-ray photoelectron spectroscopy (XPS) was carried out on a Thermo Scientific NEXSA G2 with an electron flood gun and a scanning ion gun. The spectra were collected using an ultrahigh vacuum (UHV) apparatus with a base pressure below 1×10^{-10} Pa. To prepare the XPS sample, the symmetric coin cell was charged/discharged with a current density of 1.0 mAcm^{-2} and stopped at the stripping state. The lithium anode was rinsed with DME (BASF Corp) solvent to remove the electrolyte residuals after disassembling in the glovebox and then dried at room temperature in glovebox. All the data were calibrated using the C 1s peak at 284.8 eV.

Supporting Information

Supporting Information is available from the Wiley Online Library or from the author.

Acknowledgements

Materials synthesis and battery tests were performed at the Energy Storage Lab, Materials Science and Engineering Department, University of Wisconsin-Milwaukee (UWM). XRD and N_2 adsorption/desorption isotherms were done at the Advanced Analysis Facility (AAF), UWM. SEM imaging was carried out at the Electron Microscopy Lab of the UWM Biology Department. XPS tests were performed using the facility of the NUANCE Center at Northwestern University. This work was supported by the NSF grant #2013525.

Conflict of Interest

The authors declare no conflict of interest.

Author Contributions

J.J.N. conceived the project. O.S. and F.Y.W. prepared multilayer $Ti_3C_2T_x$ MXene samples. O.S. synthesized all the other samples and performed the characterizations and battery performance tests. J.J.N. and O.S. wrote the manuscript. All authors participated in the data discussion.

Data Availability Statement

The data that support the findings of this study are available from the corresponding author upon reasonable request.

Keywords

coating, covalent organic framework, dendrite suppression, lithium metal battery, MXenes

Received: February 11, 2025
Revised: April 3, 2025
Published online: April 30, 2025

[1] B. Dunn, H. Kamath, J. M. Tarascon, *Science* **2011**, *334*, 928.
[2] D. Lin, Y. Liu, Y. Cui, *Nat. Nanotechnol.* **2017**, *12*, 194.
[3] C. Wei, Y. Wang, Y. Zhang, L. Tan, Y. Qian, Y. Tao, S. Xiong, J. Feng, *Nano Res.* **2021**, *14*, 3576.
[4] Y. Xie, H. Zhang, J. Yu, Z. Liu, S. Zhang, H. Shao, Y. Cao, X. Huang, S. Li, *Small* **2022**, *18*, 2104876.
[5] L. L. Kong, L. Wang, Z. C. Ni, S. S. Liu, G. R. Li, X. P. Gao, *Adv. Funct. Mater.* **2019**, *29*, 1808756.
[6] X. J. Liu, J. Liu, T. Qian, H. L. Chen, C. L. Yan, *Adv. Mater.* **2020**, 32.
[7] Y. M. Zhao, G. X. Li, Y. Gao, D. W. Wang, Q. Q. Huang, D. H. Wang, *ACS Energy Lett.* **2019**, *4*, 1271.
[8] P. B. Zhai, L. X. Liu, Y. Wei, J. H. Zuo, Z. L. Yang, Q. Chen, F. F. Zhao, X. K. Zhang, Y. J. Gong, *Nano Lett.* **2021**, *21*, 7715.
[9] C. B. Jin, T. F. Liu, O. W. Sheng, M. Li, T. C. Liu, Y. F. Yuan, J. W. Nai, Z. J. Ju, W. K. Zhang, Y. J. Liu, Y. Wang, Z. Lin, J. Lu, X. Y. Tao, *Nat. Energy* **2021**, *6*, 378.
[10] X. D. Ren, L. F. Zou, S. H. Jiao, D. H. Mei, M. H. Engelhard, Q. Y. Li, H. Y. Lee, C. J. Niu, B. D. Adams, C. M. Wang, J. Liu, J. G. Zhang, W. Xu, *ACS Energy Lett.* **2019**, *4*, 896.
[11] Y. Gu, J. Hu, M. Lei, W. Li, C. Li, *Adv. Energy Mater.* **2024**, *14*, 2302174.
[12] C. Wang, W. Li, Y. Jin, J. Liu, H. Wang, Q. Zhang, *Small* **2023**, *19*, 2300023.
[13] X. Zeng, M. Mahato, W. Oh, H. Yoo, V. H. Nguyen, S. Oh, G. Valurouthu, S. K. Jeong, C. W. Ahn, Y. Gogotsi, I. K. Oh, *Energy Environ. Mater.* **2024**, *7*, 12686.
[14] Z. Zhao, W. Chen, S. Impeng, M. Li, R. Wang, Y. Liu, L. Zhang, L. Dong, J. Unruangsri, C. Peng, C. Wang, S. Namuangruk, S. Y. Lee, Y. Wang, H. Lu, J. Guo, *J. Mater. Chem. A* **2020**, *8*, 3459.
[15] S. Wang, Q. Wang, P. Shao, Y. Han, X. Gao, L. Ma, S. Yuan, X. Ma, J. Zhou, X. Feng, B. Wang, *J. Am. Chem. Soc.* **2017**, *1392017*, 4258.

[16] X. Chen, Y. Li, L. Wang, Y. Xu, A. Nie, Q. Li, F. Wu, W. Sun, X. Zhang, R. Vajtai, *Adv. Mater.* **2019**, *31*, 1901640.
[17] Y. W. Song, P. Shi, B. Q. Li, X. Chen, C. X. Zhao, W. J. Chen, X. Q. Zhang, X. Chen, Q. Zhang, *Matter* **2021**, *4*, 253.
[18] X. Wu, S. Zhang, X. Xu, F. Wen, H. Wang, H. Chen, X. Fan, N. Huang, *Angew. Chem., Int. Ed.* **2024**, *63*, 202319355.
[19] X. Fan, Y. Zhang, Y. Dou, X. Li, Z. Zhao, X. Zhang, H. Wu, S. Qiao, *ACS Appl. Mater. Interfaces* **2023**, *15*, 51694.
[20] S. Zheng, Y. Fu, S. Bi, X. Yang, X. Xu, X. Li, Q. Xu, G. Zeng, *Angew. Chem., Int. Ed.* **2025**, *64*, 202417973.
[21] X. Chen, M. W. Shang, J. Niu, *Nano Lett.* **2020**, *20*, 2639.
[22] M. Shang, O. G. Shovon, F. E. Y. Wong, J. Niu, *Adv. Mater.* **2023**, *35*, 2210111.
[23] Z. Wang, S. Qin, F. Chen, S. Chen, D. Liu, D. Jiang, P. Zhang, P. M. Santiago, D. Hegh, P. Lynch, A. S. Alotabi, G. G. Andersson, P. C. Howlett, M. Forsyth, W. Lei, J. M. Razal, *ACS Nano* **2024**, *18*, 3531.
[24] C. Liu, Z. Yuan, K. Chen, Y. Jiang, M. Yue, K. Dong, Y. Liu, Y. Guo, Y. Wang, *ACS Appl. Mater. Interfaces* **2023**, *15*, 56356.
[25] H. Shi, C. J. Zhang, P. Lu, Y. Dong, P. Wen, Z. S. Wu, *ACS Nano* **2023**, *13*, 14308.
[26] M. Naguib, M. Kurtoglu, V. Presser, J. Lu, J. J. Niu, M. Heon, L. Hultman, Y. Gogotsi, M. W. Barsoum, *Adv. Mater.* **2011**, *23*, 4248.
[27] A. P. Cote, A. I. Benin, N. W. Ockwig, M. O'Keeffe, A. J. Matzger, O. M. Yaghi, *Science* **2005**, *310*, 1166.
[28] L. Kong, Y. Li, C. Peng, L. Sun, K. Wang, Y. Liu, W. Feng, *Nano Energy* **2022**, *104*, 107905.
[29] W. Liu, P. Zhai, S. Qin, J. Xiao, Y. Wei, W. Yang, S. Cui, Q. Chen, C. Jin, S. Yang, Y. Gong, *J. Energy Chem.* **2021**, *56*, 463.
[30] D. N. Hendrickson, J. M. Hollander, W. L. Jolly, *Inorg. Chem.* **1970**, *9*, 612.
[31] X. Y. Zhang, A. X. Wang, X. J. Liu, J. Y. Luo, *Acc. Chem. Res.* **2019**, *52*, 3223.
[32] M. Cui, H. Zhao, Y. Qin, S. Zhang, R. Zhao, M. Zhang, W. Yu, G. Gao, X. Hu, Y. Su, K. Xi, S. Ding, *Energy Environ. Mater.* **2024**, *7*, 12659.
[33] M. Heidari, M. Solimannejad, *Phys. B:Condens. Matter* **2023**, *664*, 415027.
[34] F. Shahzad, A. Iqbal, H. Kim, C. M. Koo, *Adv. Mater.* **2020**, *32*, 2002159.
[35] R. Wang, H. Lyu, G. S. H. P. Ho, H. Chen, Y. Yuan, K. T. Bang, Y. Kim, *Small* **2024**, *20*, 2306634.
[36] H. Zhang, X. Liao, Y. Guan, Y. Xiang, M. Li, W. Zhang, X. Zhu, H. Ming, L. Lu, J. Qiu, Y. Huang, G. Cao, Y. Yang, L. Mai, Y. Zhao, H. Zhang, *Nat. Commun.* **2018**, *9*, 3729.
[37] A. Lipatov, H. Lu, M. Alhabeb, B. Anasori, A. Gruverman, Y. Gogotsi, A. Sinitskii, *Sci. Adv.* **2018**, *4*, aat0491.
[38] J. Sun, A. Iakunkov, I. A. Baburin, B. Joseph, V. Palermo, A. V. Talyzin, *Angew. Chem.* **2020**, *59*, 1087.
[39] W. Wang, Z. Yang, Y. Zhang, A. Wang, Y. Zhan, L. Chen, Q. Li, S. Qiao, *Energy Storage Mater.* **2022**, *46*, 374.
[40] D. Zhang, S. Wang, B. Li, Y. Gong, S. Yang, *Adv. Mater.* **2019**, *31*, 1901820.
[41] X. Yang, J. Mao, H. Niu, Q. Wang, K. Zhu, K. Ye, G. Wang, D. Cao, J. Yan, *Chem. Eng. J.* **2021**, *406*, 126713.
[42] K. Yan, B. Sun, P. Munroe, G. Wang, *Energy Storage Mater.* **2018**, *11*, 127.
[43] M. Shang, X. Chen, J. Niu, *Cell Rep. Phys. Sci.* **2022**, *3*, 100767.